



Research Paper

Automatic acquisition, analysis and wilting measurement of cotton 3D phenotype based on point cloud



Haoyuan Hao^{a,b,c,d,1}, Sheng Wu^{b,c,1}, YuanKun Li^{b,c,e}, Weiliang Wen^{b,c}, jiangchuan Fan^{b,c}, Yongjiang Zhang^e, Lvhan Zhuang^{a,b,c,d}, Longqin Xu^{a,d}, Hongxin Li^{a,d}, Xinyu Guo^{b,c,*}, Shuangyin Liu^{a,d,**}

^a College of Information Science and Technology, Zhongkai University of Agriculture and Engineering, Guangzhou, 510225, China

^b Information Technology Research Center, Beijing Academy of Agriculture and Forestry Sciences, Beijing, 100097, China

^c Beijing Key Lab of Digital Plant, National Engineering Research Center for Information Technology in Agriculture, Beijing, 100097, China

^d Guangzhou Key Laboratory of Agricultural Products Quality & Safety Traceability Information Technology, Zhongkai University of Agriculture and Engineering, Guangzhou, 510225, China

^e State Key Laboratory of North China Crop Improvement and Regulation, Key Laboratory of Crop Growth Regulation of Hebei Province, College of Agronomy, Hebei Agricultural University, Baoding, 071001, China

ARTICLE INFO

ABSTRACT

Keywords:

Phenotypic analysis

Deep learning

Leaf wilting

Multi-view

This study constructed a high-throughput method for the acquisition and analysis of three-dimensional phenotypes of cotton, and proposes a method for evaluating the degree of wilting of cotton varieties based on phenotype. The upgraded version of the self-developed data acquisition platform MVS-Pheno V2 was used to continuously collect point cloud data. PointSegAt deep learning network model was used to establish plant stem and leaf segmentation and leaf overlap distinction models, realising the segmentation of cotton plant stems and leaves and the distinction of leaf overlap. In addition, an algorithm called "Active Boundary Segmentation" has been developed, which achieved automatic segmentation of overlapping cotton leaves. Based on point cloud technology, the automation of plant height, leaf count, and wilted leaf area based on voxels was realised, and a set of wilt measurement methods for cotton plants was designed. The results show that the PointSegAt model proposed has good performance in stem and leaf segmentation, with a segmentation accuracy of 0.995 and mean intersection over union of 0.924. In terms of single leaf segmentation, the average accuracy reached 0.95, and the average f1-score reached 0.94. Compared with manual measurements of plant height, leaf count, leaf area, and canopy area, the correlation coefficients were 0.99, 0.96, 0.90, and 0.99, respectively, and the root mean square errors were 0.01, 0.04, 0.19, and 0.02, respectively. Finally, the proposed method was used to perform wilting quantification experiments on two different varieties of cotton plants, and quantitative analysis of drought resistance of different varieties was conducted.

1. Introduction

Cotton is an important crop that provides valuable raw material for the global textile industry. However, abiotic stresses, especially water scarcity, have severely affected cotton production. (Aslam et al., 2023). In this context, the study of plant phenotypes becomes crucial. Plant phenotyping is a comprehensive quantitative evaluation of complex traits such as development, growth, resistance, tolerance, physiology,

structure, yield and ecology. Traditionally, obtaining phenotypic data mainly relies on manual measurements, which is not only labour-intensive but also inefficient. Fortunately, with the rapid development of high-throughput phenotyping platforms and phenotyping technologies in recent years, the efficiency and throughput of phenotypic data acquisition have been greatly improved. In particular, the application of intelligent algorithms for phenotyping based on deep learning frameworks has made possible the intelligence of phenotyping technologies and their related hardware and software systems. These

* Corresponding author. Information Technology Research Center, Beijing Academy of Agriculture and Forestry Sciences, Beijing, 100097, China.

** Corresponding author. College of Information Science and Technology, Zhongkai University of Agriculture and Engineering, Guangzhou, 510225, China.

E-mail addresses: guoxy73@163.com (X. Guo), shuangyinliu@126.com (S. Liu).

¹ Haoyuan Hao and Sheng Wu contributed equally to this work.

Symbols

MLP	Multilayer perceptron
Acc	Accuracy
Miou	Mean intersection over union
Pre	Precision
R ²	Coefficient of Determination
RMSE	Root Mean Square Error
RRMSE	Relative root mean square error
MAcc	Mean accuracy
SBF	Surface boundary filter

advances have provided technical support for the precise identification of crop resistance and stress tolerance phenotypes and new possibilities for accelerating variety breeding. Therefore, the use of advanced technologies such as deep learning for plant phenotyping is of great significance for improving cotton yields and agricultural production in general. (Gill et al., 2022).

Cotton is a multibranched structurally complex plant with large, rounded leaves that can easily cause overlap and occlusion. Cotton growth is largely dependent on moisture content, and drought can negatively affect cotton yield, root proliferation, and resistance to diseases and pests. High temperatures and water stress seriously affect cotton production. In recent years, with the development of sensor technology, research on pest detection based on image, CT, hyperspectral and multispectral technologies has been increasing. (Lin et al., 2023; Zhang et al., 2023). Cotton wilt (Yang et al., 2022), plant drought stress (Choudhury et al., 2023; Li, Wen, et al., 2022), root-knot nematode (Ramamoorthy et al., 2022), and waterlogging stress (Zhao et al., 2021) have been intensively investigated by using hyperspectral techniques. By analysing data such as plant physiological characteristics, spectral features and reflectance, various algorithms and models were used to achieve early disease detection and stress level assessment. In addition, image processing and machine learning techniques have been used to identify water stress in different crops (e.g. peanut, tomato, maize and soybean). By analysing image colour spatial indices (Sarkar et al., 2021), digital features (Chandel et al., 2021; Laxman et al., 2022; Zhou, Zhou, et al., 2021), multispectral imaging (Zhou, Zhou, et al., 2021), and RGB-D data (Qiu et al., 2021), plant stress levels and resistance. However, there are many limitations in obtaining phenotypes based on a two-dimensional scale. Due to the complex structure of most plants with problems such as shading, overlapping, and multiple branches, it is difficult to obtain accurate parameter information based on the 2D scale alone. Therefore, further research and technological innovations are needed to solve these problems and improve the accuracy of phenotype acquisition.

In recent years, researchers have opened up new perspectives for plant phenotype identification and yield prediction through innovative 3D point cloud technologies and deep learning methods. Researchers have used different approaches to achieve plant point cloud segmentation, such as developing a top-down point cloud segmentation algorithm for maize seedlings using optimal transmission distance and a semi-automatic point cloud segmentation tool, Label3DMaize, to achieve fine point cloud segmentation and labelling (Miao et al., 2021). They integrated a high-throughput data acquisition and deep learning point cloud segmentation technology, DeepSeg3DMaize, to automatically segment stem, leaf and organ instars and extract multiple phenotypic features based on them (Li, Wen, et al., 2022). They also proposed a point cloud down-sampling strategy: the VFPS based on the deep learning method PSegNet (Li, Wen, et al., 2022).

In cotton, they used ground-based LiDAR technology to acquire high-resolution 3D point clouds of plants under field conditions and developed a data processing workflow. The workflow extracts the skeleton

through a Laplace-based shrinkage algorithm, converts the plant skeleton point cloud into a graph to identify the main stem, and then detects the nodes by finding the intersection of the main stem and branches to extract two phenotypic features: the number of nodes and the length of the main stem (Sun et al., 2021). They improved GPhenoVision by adding a multi-angle colour imaging module and developed a Deep-Flower method based on deep learning for detecting and counting the number of plant flowers (Jiang et al., 2018). They developed a method for 3D mapping of cotton bolls in cotton gardens under field conditions. The method employs a region-based classification algorithm and a density-based clustering method to accurately estimate the number of cotton bolls even when they are in direct contact with other bolls (Jiang et al., 2020).

The development and application of these methods have not only improved the accuracy and efficiency of plant phenotypic identification, but also provided a powerful tool for the advancement of breeding techniques and the improvement of crop yields. However, for plants with complex morphology like cotton, these methods alone cannot effectively perform organ-scale segmentation.

Phenotype acquisition techniques based on 3D scales have obvious advantages in solving the problems of occlusion, overlapping and wilting. To solve the occlusion problem, researchers have proposed various segmentation methods, such as an unsupervised training method that gradually removes occluded point clouds (Wang et al., 2021), a point cloud occlusion recovery method based on shallow feed-forward neural networks (Barazzetti, 2018), and an occlusion detection method based on voxel ray-tracing techniques (Hirt et al., 2022). These methods have proved to be highly accurate and stable in dealing with high-density point clouds with occlusion problems.

Early methods to solve the overlap problem mainly include segmenting the overlapping parts by alignment algorithms (Xiao et al., 2013), octree-based region growing (Vo et al., 2015), and so on. In recent years, new approaches to solving the overlap problem include alignment networks based on intermediate unaligned images between two low overlapping point clouds. By learning triple depth features and two-stage classifiers for different modalities, an accurate rigid transformation can be created in the overlapping region (Chen, Wei, Xu, Wei, & Wang, 2022 b , July). There is also research on segmentation of individual trees and plant leaves in forest scenes. Tree segmentation and extraction in dense forests and overlapping canopies were achieved by semantic segmentation module, instance segmentation module and post-processing refinement methods (Chang, Fan, Zhu, & Dong, 2022 a). In fruit detection and localisation research, the combination of improved F-PointNet, 3D clustering and ball-fitting methods enables accurate detection and localisation of individual ripe fruits in orchard environments. These research results are of great significance in solving the point cloud occlusion problem and improving the effectiveness of point cloud analysis and application (Li et al., 2019).

By quantifying plant physiological changes and utilizing accurate 3D point cloud data of plant canopy, different drought mechanisms can be captured, and drought tolerant varieties can be selected. An end-to-end pipeline based on point clouds is used to investigate drought stress at different stages through 3D reconstruction, segmentation and feature extraction using deep neural networks. By constructing an accurate 3D model and deep network-based feature aggregation, the degree of drought stress in crops can be determined. This method is superior to traditional methods and helps to screen drought-tolerant varieties in high throughput (Liu et al., 2020).

These studies provide important technical support for organ-scale segmentation, phenotype extraction, selection of drought-tolerant varieties, and smart irrigation. However, relatively limited studies have been conducted to acquire data using multi-view imaging techniques and to assess the degree of wilting and select drought-tolerant varieties in complex plants such as cotton and peanut using 3D point clouds. Therefore, using cotton under drought stress as a data source, a 3D point cloud acquisition device suitable for complex plants was investigated. In

addition, a point cloud-based method for automatic assessment of wilt degree and phenotype extraction was developed. The main contributions of this study are as follows.

1. Tackle the challenge of acquiring complex plant point cloud data - upgrading multi-view acquisition equipment.
2. Solving the problem of complex plant organ segmentation - Introducing an organ-level segmentation method for cotton.
3. Automatic phenotype calculation and wilt measurement
4. Development of a Cotton MVS software package

2. Materials and methods

This study introduces an automated analysis framework for the three-dimensional reconstruction of cotton wilting degree and phenotype extraction based on multi-view images. Fig. 1 outlines the specific process from data acquisition to software (Cotton MVS). A represents the acquisition and reconstruction of multi-view images, B represents data preprocessing, C denotes semantic segmentation based on PointSegAt, which is used for stem and leaf segmentation, D represents leaf instance segmentation based on active boundary segmentation (ABS), and E represents wilting degree measurement and phenotype extraction. Finally, an automated phenotype acquisition software (Cotton MVS) was developed based on the above methods, and these steps will be detailed in the following sections.

2.1. Material

In this experiment, two cotton varieties, Jnd36 and J2658, were planted in April 2022 in the dry shed of Beijing Academy of Agriculture and Forestry. Three levels of water stress were applied to these two varieties at different growth stages. The growing environment is shown in Fig. 2. Seedling treatments included.

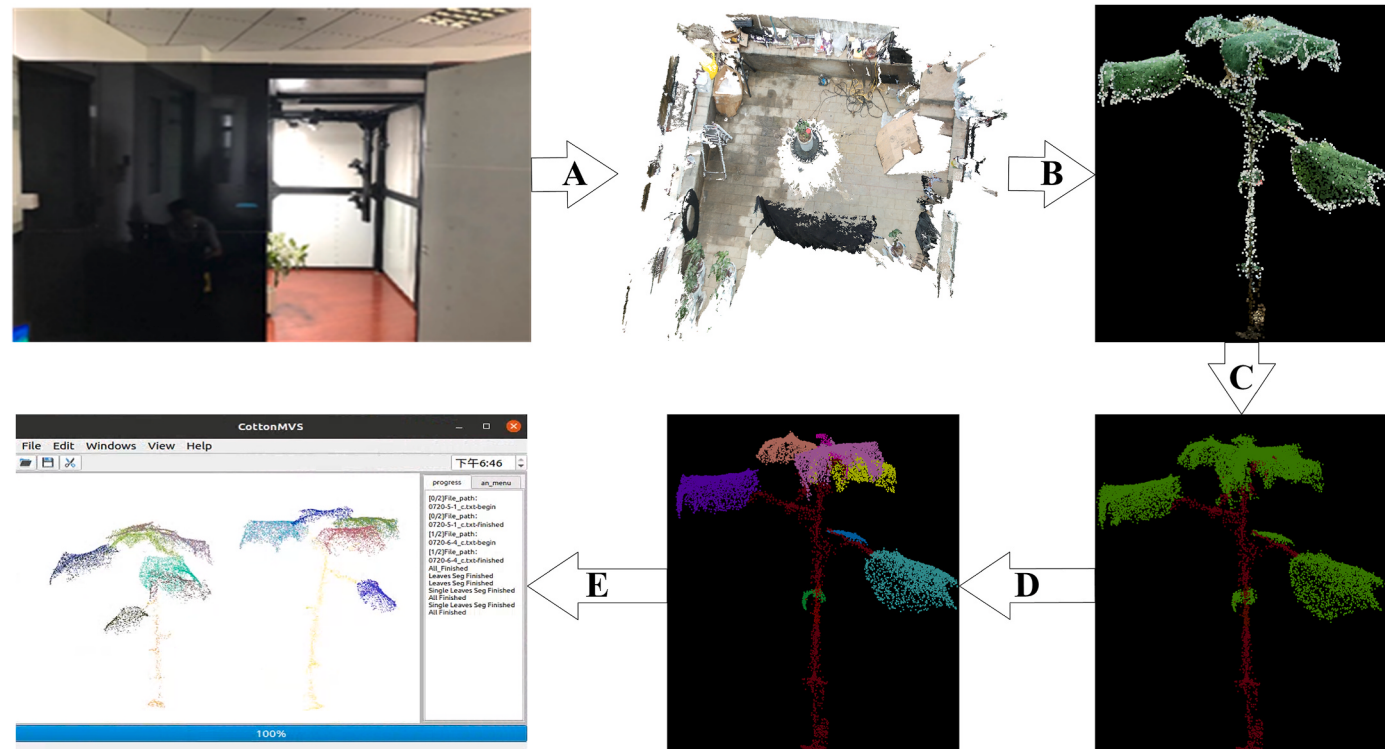


Fig. 1. Acquisition and Reconstruction of Multi-View Images. A) acquisition and reconstruction of multi-view images, B) data pre-processing, C) semantic segmentation based on PointSegAt for stem and leaf segmentation, D) leaf instance segmentation based on Active Boundary Segmentation (ABS), and E) wilting measurements and phenotypic extraction.

- a. Severe drought, i.e., cessation of irrigation from the three-leaf stage, resulting in a drop in soil moisture to severe drought levels (<45 per cent);
- b. Moderate drought, i.e., cessation of irrigation from the three-leaf stage, resulting in a decline in soil moisture and maintaining it at the moderate drought level (50 ± 5 per cent);
- c. Mild drought, where small amounts of water are provided throughout to ensure mild drought stress ($75 \pm 5\%$).

Humidity returned to normal levels after 20 days in all drought treatments.

The treatments at seedling and bud stage were as follows: prior to bud stage, cotton plants were managed normally without water stress. Then, water treatments were initiated at the bud stage, including.

- Severe drought, where irrigation is stopped from the germination stage, resulting in soil moisture dropping to severe drought levels;
- Moderate drought, where irrigation is discontinued from the germination stage, resulting in a decrease in soil moisture and maintaining it at a moderate drought level;
- Mild drought, where small amounts of water are provided throughout to ensure mild drought stress ($75 \pm 5\%$).

These treatments also included a return of moisture to normal levels after 20 days. Specifically, it was possible to study the effects of different levels of water stress on two cotton varieties at different growth stages. The stress levels are shown in Table 1.

2.2. Data collection

2.2.1. Data collection platform

Data were collected using an upgraded version of the MVS-PhenoV2 platform (Wu, Wen, Lan, et al., 2022). The device was optimised over its predecessor in terms of light source, sensors and box design. The top of



Fig. 2. Planting environment of experimental materials.

Table 1

Degree of water stress of experimental materials. The degree of water stress of experimental materials started from the three-leaf stage in the seedling stage and from the day of budding in the bud stage.

Period	Treatment method		
	Mild drought (%)	Moderate drought (%)	Severe drought (%)
Germination stage	75	50	45
Seedling stage	75	50	45
Bud stage	75	50	45

the box is equipped with four incandescent lights for even illumination. An overhead camera has also been added to capture more detail and provide support for plants with more complex canopy structures. A rod on the right side supports the three adjustable RGB cameras. The height of each camera is freely adjustable as shown in Fig. 3b Module b. Each camera is equipped with a separate telescopic platform for adjusting the horizontal position of the camera. The improved platform is more suitable for plants of different sizes. The device still uses the multi-view imaging technique to acquire point cloud data. With this device, point cloud data with consistent density were obtained, which laid the foundation for subsequent experiments. The data acquisition process is shown in Fig. 3a, and the structure of the device is shown in Fig. 3b.

2.2.2. Data acquisition

The data collection started on June 1, 2022 and ended on July 26, 2022, when a total of 300 point cloud datasets were collected from different cotton varieties at different times as shown in Table 2 below. As shown in Table 2, a total of 300 point cloud datasets were collected from different cotton varieties at different times. These included 150 plants

Table 2

Detailed information on data collection.

Variety	Period			
	Emergence period	Seedling stage	Budding stage	Summary
Jnd36	50	50	50	150
J2658	50	50	50	150
Summary	100	100	100	300

each of Jnd36 and J2658. Fifty plants were collected at seedling, bud and flowering stages. The data were collected continuously using an alternate day data collection strategy.

For the acquired data, the background and flower pots are first removed to obtain a single plant point cloud. However, due to the high number of interfering factors in the reconstruction process, there is a large amount of noise in the single plant point cloud. A denoising algorithm is used to denoise the point cloud to obtain the final plant point cloud. The specific process is shown in Fig. 1A, with the red point cloud representing noise. Finally, the collected data were labelled. The labelling was done using Cloud Compare software (Girardeau-Montaut, 2016) with a binary classification, with stems and leaves in each category. The labelled data were divided into a training set, a test set and a validation set in a ratio of 7:2:1. This lays a solid foundation for subsequent experiments.

2.3. Method

2.3.1. Stem and leaf segmentation based on PointSegAt

Referring to the concept of PointNet++ MSG (Qi et al., 2017a), the PointSegAt network for stem-and-leaf segmentation was designed. PointSegAt consists of five main components: radius interpolation, grouping and down-sampling, weighted interpolation, interpolation

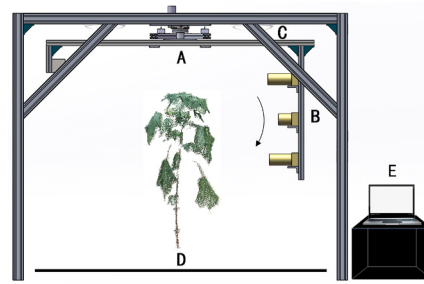
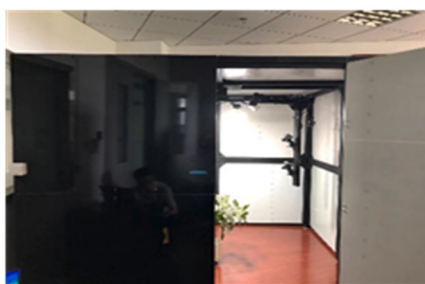


Fig. 3. Data collection and structure diagram of the collection device. Data collection and structure diagram of the collection device, the left figure shows the data collection flowchart, the right figure shows the structure diagram of the collection device. A represents the electric motor, B represents the RGB camera, C represents the incandescent lamp, D represents the carpet, and E is the main control computer.

operation, and attention mechanism. The network structure is shown in Fig. 4. The input consists of point cloud data containing only position and label information. Radius interpolation utilises a module of PointNet++ with the aim of extracting and abstracting features from the input point cloud data in a hierarchical manner in order to better capture local and global features. Grouping and down-sampling are used to down-sample and merge surrounding point information to enhance local feature extraction. Weighted interpolation uses weighted computation for interpolation and up-sampling of local point clouds. The attention mechanism enhances the feature learning capability. The following section describes each module in detail.

Radius Interpolation For all input points, the Euclidean squared distance between two points is calculated and it is determined if the distance is greater than the input radius value. If the distance is greater than the radius value, set the distance to a large value, chosen in this experiment to be 1024. Then sort the array of distances. If the distance is within the radius, it is checked to see if it satisfies the number of points threshold N. If not, the first point is populated until the threshold is satisfied. The points are then fed into the multilayer perceptron (MLP). If the threshold is satisfied, the points are fed directly into the MLP. the process is shown in Fig. 4A.

Grouping and Down-sampling The input points are sampled at the farthest point, grouped to enhance the local features, and then passed through the MLP to get the calculated new point array. The operation is shown in Fig. 4B.

Weighted Interpolation For all input points, the distance between two points is calculated and weights are calculated based on these distances. Then interpolation is done based on the weights and finally a new point array is generated. The whole process is shown in Fig. 4C.

Interpolation Operation Select the corresponding number of points for the input.

Attention Mechanism The specific implementation is as follows.

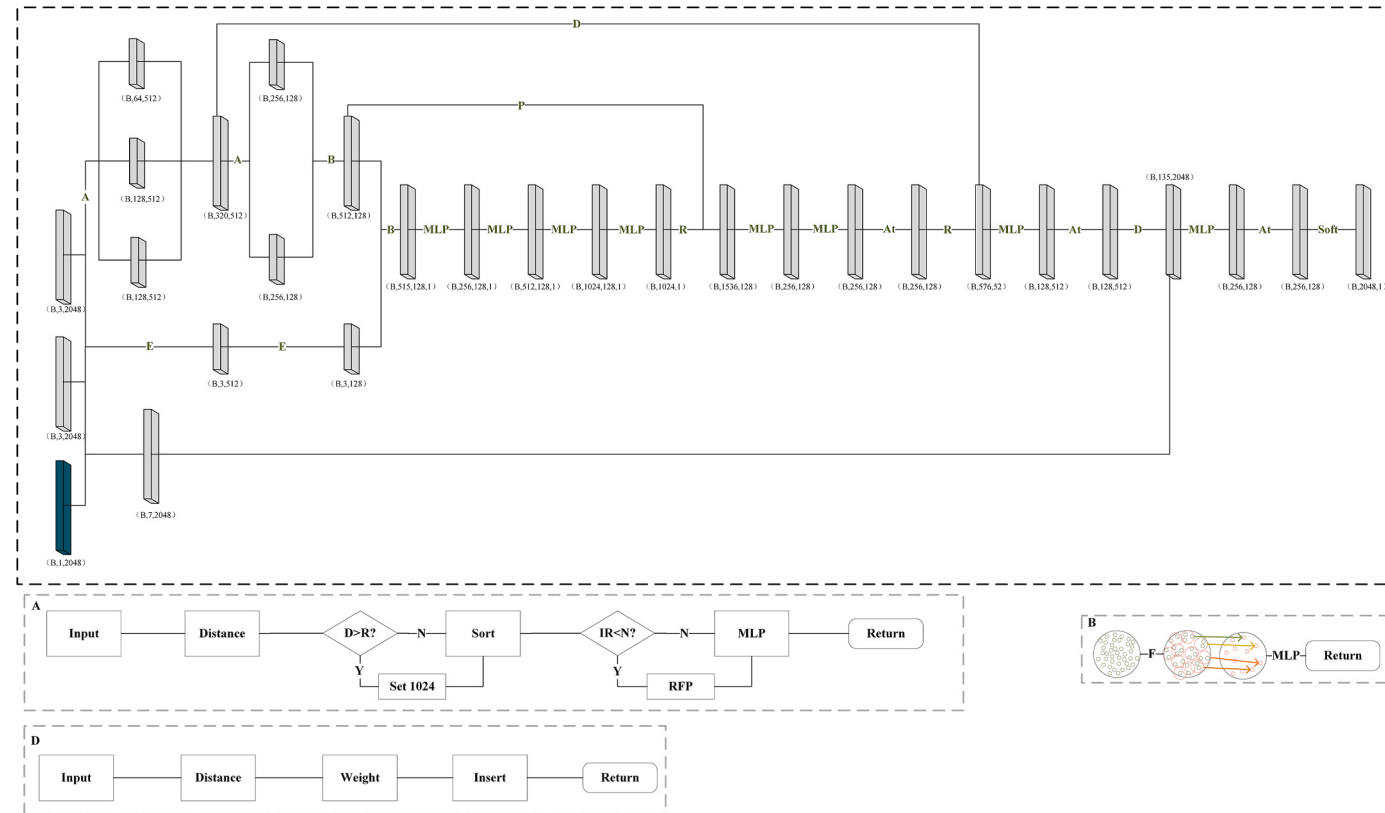


Fig. 4. Illustration of the model and modules of the PointSegAt network. A) radius interpolation; B) grouping and downsampling; D) weighted interpolation; E) interpolation operation. At is the attention mechanism; MLP (Multi-Layer Perceptron): a neural network layer used for feature extraction and transformation, P (Permute): p (Permute): an operation that arranges dimensions; R (Repeat): Repeat operation.

Assume the input feature is x , where the dimension of x is (B, C, L) . B represents batch size, C represents the number of channels, and L represents the feature length. Firstly, through the linear transformation operations of query, key, and value, the corresponding query vector q , key vector k , and value vector v are obtained. The formulas are as follows:

$$q = W_q \times x \text{ (dimension :}(B, C / 8, L)\text{)}$$

$$k = W_k \times x \text{ (dimension :}(B, C / 8, L)\text{)}$$

$$v = W_v \times x \text{ (dimension :}(B, C, L)\text{)}$$

where W_q , W_k , W_v represent the corresponding convolution kernel weights, // represents integer division, discarding the decimal part.

Then, calculate the attention weight:

$$attn = softmax(q^T \times k) \text{ (dimension :}(B, L, L)\text{)}$$

Where T represents the transpose operation.

Next, multiply the calculated attention weight $attn$ with the value vector v to get the adjusted value of the feature.

$$out = v \times attn \text{ (dimension :}(B, C, L)\text{)}$$

Finally, add the adjusted value 'out' to the original feature 'x', and adjust it by multiplying it with the attention weight parameter γ to get the final output of the feature after weight adjustment:

$$output = \gamma \times out + x \text{ (dimension :}(B, C, L)\text{)}$$

where γ is the learned attention weight parameter (dimension is (1)).

2.3.2. ABS single leaf segmentation

Active Boundary Segmentation (ABS): Fig. 5 shows the overall flowchart of the ABS algorithm. For the leaf set obtained above, single and complex leaves were first obtained using the region growing algorithm, and then a classification network based on PointNet++ (Qi et al., 2017a) was trained using the leaves obtained by region growing (Li et al., 2018), as shown in Fig. 5A. This classification network ensures the consistency of the algorithm, and for the identified complex leaves, an edge erosion algorithm (EEA) is designed to solve the leaf overlap problem. This algorithm first up-samples the leaves to ensure that no large voids appear in the point cloud, and then segments the overlapping leaves. This method is described in detail in the following section, and the specific process is shown in Fig. 5.

Region growing: The initial seed point is chosen to be the point with the least curvature, as the region around the point with the least curvature tends to be the smoothest. Starting the region growing algorithm from the smooth region helps to reduce the total number of segmented segments, thus increasing efficiency. The steps of the algorithm are as follows.

- (1) The selected points are added to the seed set.
- (2) For each seed point, find its k nearest neighbors. The value of k is set to 15
- (3) Calculate the angle between the normal of each neighboring point and the normal of the current seed point. If the angle is less than a threshold, include the point in the current region. The angle threshold is set to 18° .
- (4) Calculate the curvature of each neighboring point. If the curvature is less than a curvature threshold, add the point to the seed set. The curvature threshold is set to 0.15.
- (5) Remove the current point from the seed set.
- (6) If the seed set is empty, end the process; otherwise, repeat the above steps.

PointNet++ Classification: For single and overlapping leaves obtained through area growth, data enhancement techniques including inversion, up-sampling, down-sampling and cropping were applied. This process produced a total of 1800 single leaves and 1780 leaves with overlapping features. These data were divided into training, test and validation sets in a ratio of 7:2:1 and trained for 1200 calendar elements using the PointNet++ classification (Qi et al., 2017a) network. The algorithm ensures continuity and segmentation accuracy. As shown in Fig. 5A, this part is only used to train the classifier and acts as an ABS in distinguishing between single and compound leaves.

Edge Erosion Algorithm (EEA): in order to ensure sufficient homogeneity of the data without visible voids, complex blades are initially up-sampled. The up-sampling method involves uniform interpolation

between two points. For overlapping up-sampled blades, the EEA algorithm is designed as follows.

- (1) To avoid being affected by point cloud holes, the original point cloud was initially up-sampled to mitigate the impact of voids on segmentation accuracy, as depicted in the Raw Data block in Fig. 6;
- (2) A KD-Tree is constructed for the up-sampled data, and the K-Nearest Neighbors of the reference point X_i are found to form the point set S . The value of K is determined to be 60;
- (3) The three main direction vectors of S are calculated using the PCA algorithm, which are the normal vector n and two direction vectors u, v . ($n \perp u \perp v$);
- (4) A vector V_{ij} is formed by selecting a point j from the point set S with respect to i , then use u and v to form plane P , project vector V_{ij} onto P to form vector V_{ij}^{uv} , θ is the angle between V_{ij}^{uv} and vector u , and construct the angle set θ_{all} ;
- (5) The set θ_{all} is sorted. If the maximum angle difference $\max(\theta_{j+1} - \theta_j) > \theta_{threshold}$ or $\max(\theta_{all}) < \theta_{max}$ or $\min(\theta_{all}) > \theta_{min}$, Point i is regarded as an edge point, and it is incorporated into the set of edge points. Here, $\theta_{threshold}$ is 90° , θ_{max} is 180° , θ_{min} is 150° ;
- (6) Execute the above steps for all points in the point cloud to obtain all edge points and remove them. Initial iterations are carried out 8 times, followed by Euclidean distance clustering. The edge points are then restored to the original point cloud, and PointNet++ Classification is used for classification recognition. If complex leaves still exist, repeat the above steps count times, where $count = 8 + 5 \times n$ (n is 1, 2, 3, ...), or until all leaves are single leaves. The recovery of edge points is done using a point-point restoration method.

The above steps are detailed in Fig. 6.

2.3.3. Voxel-based leaf area calculation

Point cloud pixelisation is the process of converting an unstructured point cloud into a regular pixel grid. With voxelisation, point clouds can be processed and analysed more easily. Since leaf area is related to voxel size, number of voxels, voxel volume, and projected area, a voxel-based predictor and a projected area-based predictor were developed.

According to the result after voxelisation of the point cloud, the number of voxels is multiplied by 10–2 as the relative voxel number as shown in equation (1). The area of the voxel is multiplied by the height of the voxel as the volume of the voxel where the current point is located, and the sum of the voxel volumes of all points is used as the second predictor as shown in equation (2). The voxel volume is the cube of the voxel size and the sum of the voxel volumes is used as the third predictor as shown in equation (3). Finally, the projected area is used as

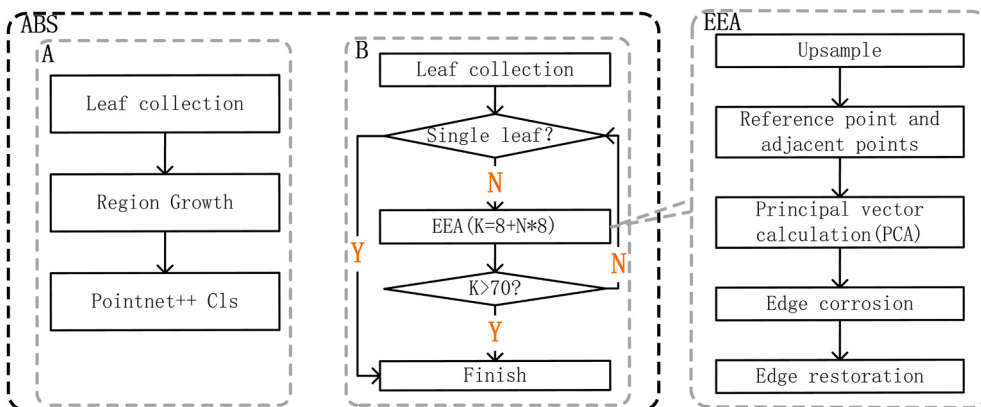


Fig. 5. Single-leaf segmentation flowchart Single-leaf segmentation flowchart, where ABS is the overall flowchart, A stands for PointNet++ classification network, B stands for single-leaf segmentation flowchart, and EEA stands for edge erosion algorithm.

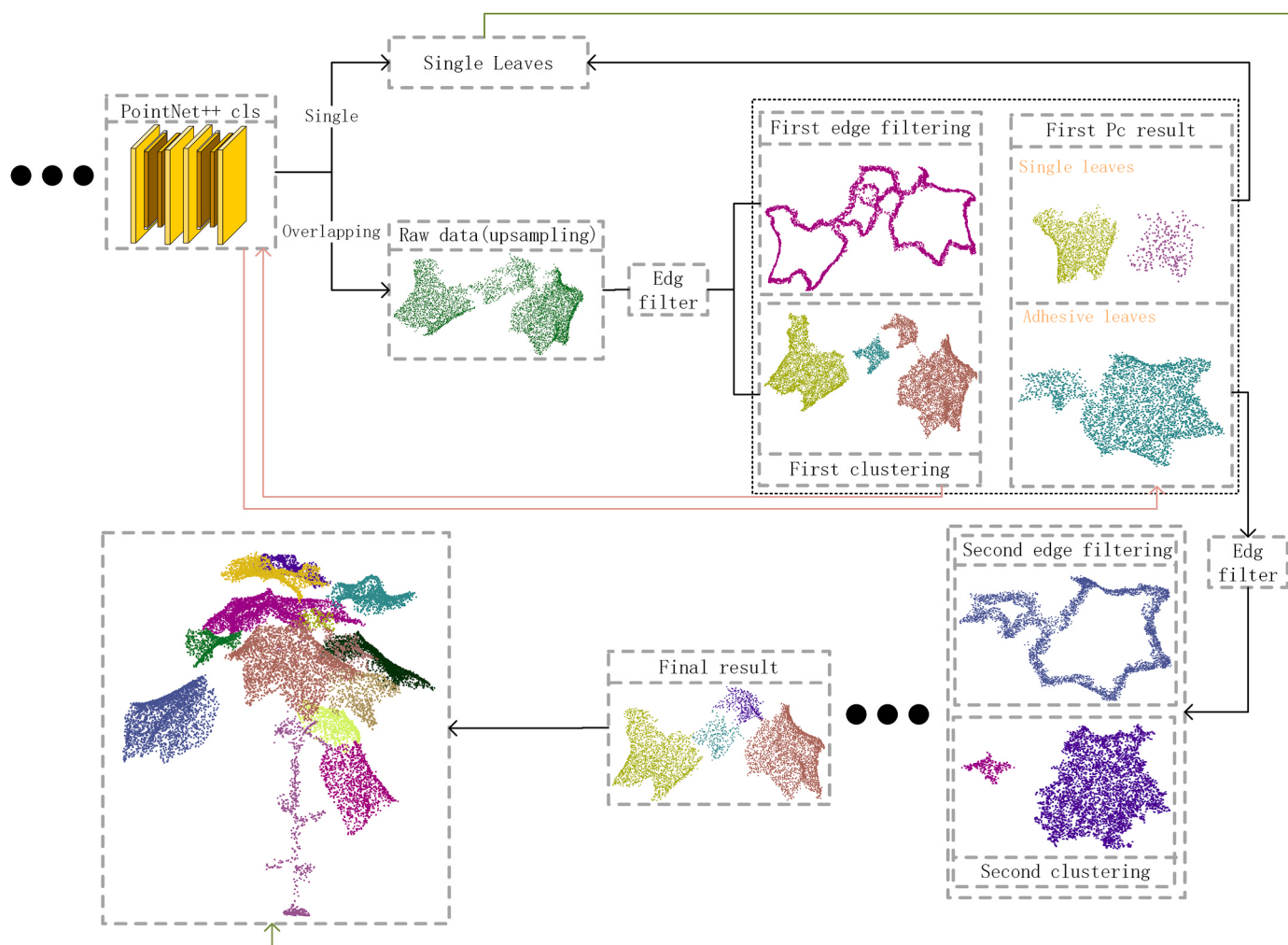


Fig. 6. Detailed description of single leaf segmentation.

the fourth predictor as shown in equation (4). These predictors can help us understand the point cloud better and improve the efficiency of point cloud processing and analysis.

$$VOX_1 = 10^{-2} \times CountofVoxel \quad (1)$$

$$VOX_2 = \sum_{i=0}^N voxel_size^2 \times (z_0 - z_1) \quad (2)$$

$$VOX_3 = \sum_{i=0}^N voxel_size^3 \quad (3)$$

$$Vox_4 = Pro_area \quad (4)$$

where *CountofVoxel* denotes the number of voxels, and *voxel_size* represents the size of the voxel, and *Pro_area* represents the projected volume

Experimental studies have shown that different voxel sizes affect the accuracy of predictions. To find the most suitable voxel size and

predictor. Maximum and minimum nearest neighbour distances were calculated for 346 leaves from 40 datasets. The minimum value was 0.1018 and the maximum value was 1.4988. Based on this, a range of voxels from 0.2 to 1.5 in increments of 0.1 was chosen and the average prediction error for each voxel size was calculated.

As shown in Table 3, the average error of different predictors varies as the voxel size gradually increases. When the voxel size is 0.9, the average errors of all predictors reach the minimum. Predictor VOX2 has the smallest mean error of 9.80. Therefore, the final voxel size of 0.9 was determined and the selected predictor was VOX2. The final predictive model is shown in equation (5). The projected leaf area was also obtained for subsequent studies. Fig. 7 illustrates the results of voxelisation of leaves with different voxel sizes.

$$Y = 70.93 \times X + 3.85 \quad (5)$$

Where *X* is the predictor, and in this study, employed VOX2 as the

Table 3

Comparison of different voxel sizes and different predictors, where $VOXi$ ($i = 1, 2, 3, 4$) represents different predictors and VoxSize represents voxel size.

Predictive	Vox_Size												
	0.2	0.3	0.4	0.5	0.6	0.7	0.8	0.9	1.0	1.1	1.2	1.3	1.4
VOX1	20.63	17.37	14.38	12.36	11.14	10.38	10.05	9.81	10.05	10.08	10.32	10.28	10.54
VOX2	20.62	17.36	14.36	12.35	11.15	10.37	10.06	9.80	10.06	10.07	10.31	10.27	10.53
VOX3	20.64	17.35	14.37	12.37	11.16	10.38	10.04	9.81	10.07	10.09	10.33	10.25	10.28
VOX4	22.00	22.00	22.00	22.00	22.00	22.00	22.00	22.00	22.00	22.00	22.00	22.00	22.00

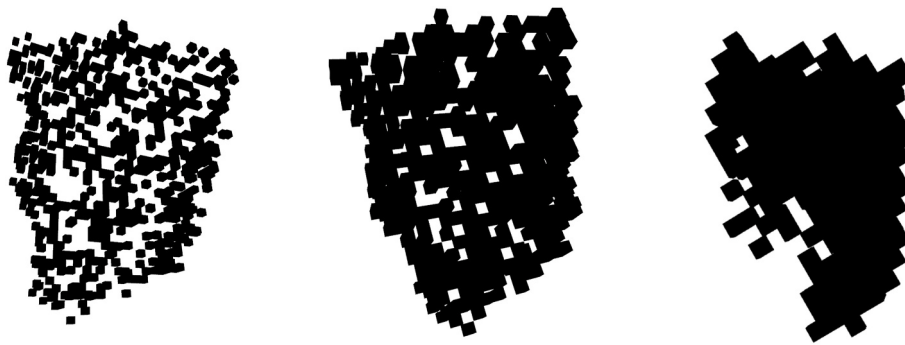


Fig. 7. Voxelisation for different voxel sizes, where A is a voxel size of 0.3, B is a voxel size of 0.6, and c is a voxel size of 0.9.

predictor.

2.3.4. Plant height, canopy area and leaf count

Plant height was determined by calculating the difference between the highest and lowest points of the plant point cloud as shown in Equation (6); canopy leaf area was recorded as the total leaf area as shown in Equation (7); and the number of leaves was the sum of segmented leaves as shown in Equation (8).

$$\text{Height} = \text{Max.Z(points)} - \text{Min.Z(points)} \quad (6)$$

where *Height* represents plant height, the *Max.Z(points)* and *Min.Z(points)* represent the maximum and minimum values of the third dimension (Z) in the input point cloud, respectively.

$$\text{Canopy Leaf Area} = \text{Sum(Area)} \quad (7)$$

Where *Canopy Leaf Area* represents the leaf area of the canopy, and *Sum(Area)* represents the sum of individual leaf areas.

$$\text{Number} = \text{Sum(Single leaf)} \quad (8)$$

Where *Number* represents the number of leaves, and *Sum(Single leaf)* represents the sum of individual leaf counts.

2.3.5. Calculation of wilting degree

Firstly, the validation data were classified according to different periods, varieties and degrees of drought stress. Then leaf area and predicted leaf area were calculated separately for each group of categorised data. The degree of wilting of individual leaves was determined based on the ratio of predicted leaf area to measured leaf area. For the leaf area of the whole plant, different weights were assigned based on the position of the leaf from top to bottom (top: middle: bottom = 6:3:1). The overall wilt was subsequently calculated from these weights. The formula for single leaf wilt is denoted in the text as (9) and for overall wilt as (10). The larger the parameter value W_{whole} parameter value, the more severe the overall wilt.

$$W_{single} = \frac{\text{Area}_{project}}{\text{Area}} \quad (9)$$

$$W_{whole} = \frac{\sum_i^i W_{single}}{i} \times 0.6 + \frac{\sum_{(k-i)}^k W_{single}}{(k-i)} \times 0.3 + \frac{\sum_{n-k-i}^n W_{single}}{(n-k-i)} \times 0.1 \quad (10)$$

Where *Area_{project}* refers to the single leaf projection area, *Area* denotes the calculated area, *i* represents the quantity of top layer blades, *k* – *i* represents the quantity of middle layer blades, and *n* – *k* – *i* represents the quantity of bottom layer blades.

2.4. Rating indicators

Accuracy (Acc) and mean intersection over union (MIou) are used for accuracy assessment of semantic segmentation. Accuracy refers to the

ratio of the number of correctly predicted samples to the total number of samples as shown in Equation (11). MIou measures the degree of overlap between the segmentation results of the model and the actual segmentation results, and denotes the mean value of the intersection over union as shown in Equation (12).

Precision (Pre), recall and f1 score are used to evaluate the accuracy of overlapping blades as shown in Eqs. (13)–(15), respectively.

The coefficient of determination (R^2) is a statistical measure used to assess the degree of fit of a regression model. It represents the proportion of the variance of the dependent variable explained by the model, as shown in equation (16).

The Root Mean Square Error (RMSE) is the square root of the mean of the squared errors in a regression model. It measures the difference between actual observations and model predictions as shown in equation (17).

The relative root mean square error (RRMSE) is a normalised version of the RMSE relative to the range of the target variable. It takes into account the variability of the target variable as shown in Equation (18).

$$\text{Accuracy} = \frac{P_T}{N} \quad (11)$$

Where P_T denotes the number of correctly predicted samples and N denotes the total number of samples.

$$\text{MIou} = \frac{1}{K} \sum_{i=1}^K \frac{\text{Intersection Area}}{\text{Union Area}} \quad (12)$$

Where K represents the number of categories, and in this study K is set to 2. *Intersection Area* refers to the area of intersection between the predicted category and the actual segmentation, *Union Area* represents the area of union between the predicted category and the actual segmentation.

$$\text{Precision} = \frac{P_{True}}{P_{True} + P_{False}} \quad (13)$$

$$\text{Recall} = \frac{P_{True}}{P_{True} + N_{False}} \quad (14)$$

Where P_{True} represents the number of samples correctly predicted as the positive category, P_{False} represents the total number of samples predicted as the positive category.

$$F1 = \frac{2 \times \text{Precision} \times \text{Recall}}{\text{Precision} + \text{Recall}} \quad (15)$$

$$R^2 = 1 - \frac{\sum_{i=1}^n (y_i - \bar{y}_i)^2}{\sum_{i=1}^n (y_i - \bar{y})^2} \quad (16)$$

Where n is the number of samples, y_i is the actual observed value, \bar{y}_i is the corresponding predicted value, \bar{y} is the mean value of the observed values.

$$RMSE = \sqrt{\frac{1}{n} \sum_{i=1}^n (y_i - y'_i)^2} \quad (17)$$

$$RRMSE = \frac{RMSE}{\max(X) - \min(X)} \quad (18)$$

Where $\max(X)$ and $\min(X)$ respectively represent the maximum and minimum values of the target variable.

3. Results

3.1. Evaluation of multi-view device

Different rotation speeds have a significant impact on the imaging quality. In addition, the number of cameras also has a significant impact on the reconstruction quality. Table 4A provides a detailed overview of the number of photos and acquisition duration for different acquisition methods. Using lower rotation speeds allows for more multi-view images to be captured, capturing more detail and thus improving the quality of the reconstructed point cloud. However, it is worth noting that more photos also imply higher resource requirements.

Different reconstruction methods have different effects on the quality and efficiency of point cloud reconstruction. We tested two different reconstruction methods: the commercial software Context Capture (Novel et al., 2016) and the open source software Open Multi-View Stereovision (OpenMVS) (Cernea 2023). As shown in Table 4B, at a rotation speed of 10, the reconstruction times for the dual-camera and triple-camera setups ranged from 190 min to 275 min and 221 min–293 min, respectively. At a rotation speed of 30, the reconstruction times for these configurations ranged from 77 to 108 min and 92–126 min, respectively. Therefore, the selection of an appropriate acquisition method is critical to ensure data quality. In this study, a three-camera setup with a rotation speed of 30 was chosen for multi-view image acquisition and 3D reconstruction using a contextual capture technique.

3.2. Semantic segmentation

PointSegAt outperformed all the corresponding networks in terms of MIou (92.4) and mean accuracy (MAcc) (99.5) (Table 5). These metrics were improved by 4.1 and 0.5, respectively, compared to the next best

Table 4

Data Acquisition Comparison. A) Different methods for acquiring image quantity and time comparison. The leftmost column indicates camera quantity/rotation speed. B) Comparison of Different Reconstruction Methods, with the last two columns indicating (reconstruction time/reconstructed point cloud points/data quality).

Table 4A

approach	project	
	Number of Images	Acquisition Duration
2/10	240	8 min
3/10	360	
2/20	120	4 min
3/20	180	
2/30	80	
3/30	120	2 min

Table 4B

approach	project	
	Context capture	OpenMVS
2/10 approach	182/18.1/A+	213/17.6/A
3/10	265/25.6/A+	285/27.3/A+
2/20	140/9.4/A	164/9.8/A-
3/20	175/11.7/A+	186/11.8/A
2/30	75/6.7/A	106/6/B
3/30	90/7.5/A+	124/6.8/B+

Table 5

Comparison of accuracy and efficiency of multi-model segmentation, where MAcc denotes the average accuracy, MIou denotes the average IoU, Train_epoch denotes the number of training calendar elements, Training_time (m) denotes the training time in minutes, and Test_time (s) denotes the test time in seconds.

	MAcc	MIou	Train_epoch	Training_time (m)	Test_time (s)
PointNet	97.8	54.7	2000	312	0.6
PointNet++ (MSG)	99.0	88.3	2000	395	1.3
Point Transformer	98.7	81.7	2000	500	1.9
KPConv	96.8	83.5	2000	375	1.0
PointSegAt (ours)	99.5	92.4	2000	385	1.2

results obtained with PointNet++. PointSegAt took 385 min to train for 2000 epochs and 1.2 s to test. Its training and testing time was the third longest of all the corresponding networks, giving the best results with limited time. PointSegAt achieved the highest accuracy and MIou despite the presence of heavy blockages and attachments at the top of the wilted cotton, which made accurate extraction difficult.

PointNet (Qi et al., 2017b) is an early point-cloud based neural network architecture that deals directly with unordered point cloud data and performs tasks such as classification, segmentation, and recognition by learning feature representations of points. PointNet++ is an extended version of PointNet that aims to enhance its ability to deal with local features and multi-scale information. It introduces a multi-level feature aggregation mechanism that improves the network's ability to model local structures by aggregating local features at different levels. The Point Transformer (Engel et al., 2021) is a point cloud processing network architecture based on a self-attentive mechanism. Unlike traditional convolutional neural networks, Point Transformer uses a self-attention mechanism that allows the network to dynamically focus on the relationships between different points as it learns point cloud feature representations. Kernel Point Convolution (KPConv) (Thomas et al., 2019) is a point cloud processing method based on kernel point convolution. Unlike traditional convolution operations, KPConv uses kernel points to dynamically adapt to the shape of the input point cloud, resulting in better handling of irregular point cloud data. Fig. 8 shows the segmentation results obtained using different methods.

3.3. Single leaf segmentation

As shown in Fig. 9, it demonstrates the segmentation results at different stages. A, B and C in Fig. 9 represent the segmentation results at seedling, growing and bud stages, respectively. The results showed that the method achieved good segmentation results at the seedling, growing and bud stage of cotton. It is worth mentioning that small leaves with less than 500 points were excluded from the leaf segmentation process, which also laid a solid foundation for the determination of wilt at the later stage.

In order to verify the segmentation effect of overlapping leaves with different complexity, the leaves are classified into four categories based on the degree of overlap: simple structures with no more than three overlapping leaves in an overlapping region (hereafter referred to as simple structures), ordinary structures with 3–4 overlapping leaves in an overlapping region (hereafter referred to as ordinary structures), and complex structures with more than five overlapping leaves in an overlapping region (hereafter referred to as complex structures). The region growing algorithm is used to segment individual leaves from the set of semantically segmented leaves.

As shown in Fig. 10, it shows the comparison results of using the Surface Boundary Filtering (SBF) (Li et al., 2019) algorithm and EEA for different overlapping blades, analysed from simple structures (A1, A2), ordinary structures (B1 to C2) and complex structures (D1, D2)

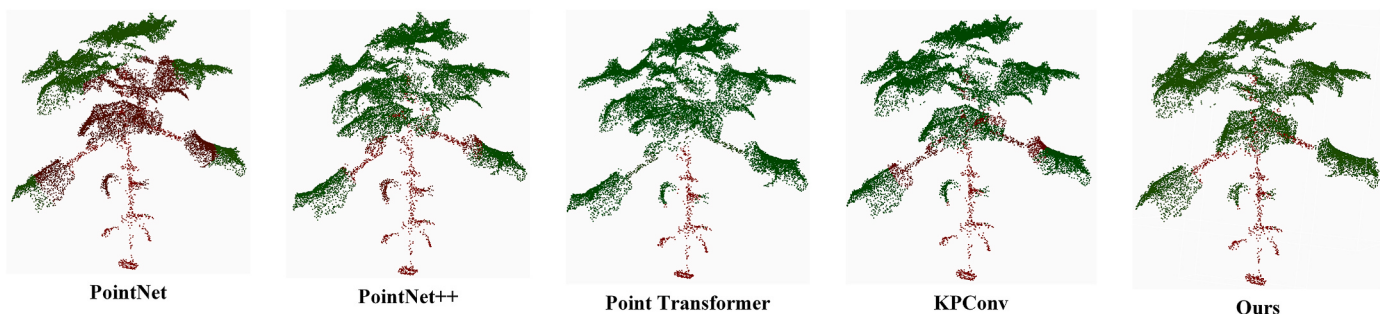


Fig. 8. Comparison of segmentation results.

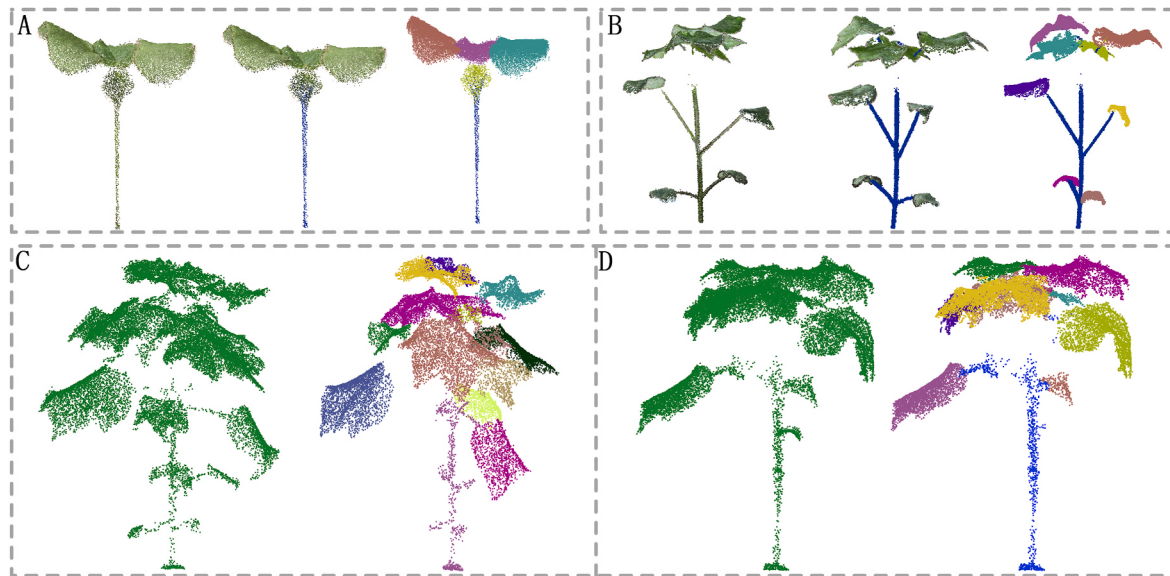


Fig. 9. Comparison of segmentation results at different stages Comparison of segmentation results at different stages, A) segmentation result at the seedling stage, B) segmentation result at the seedling stage, C and D) segmentation results at the bud stage.

respectively. From fig. A2, it can be seen that the SBF algorithm has serious mis-segmentation for the overlapping blade with holes, while EEA still segments the blade accurately, independent of the holes. figures C2 and D2 find that EEA also missegments for particularly complex leaves. For incomplete leaves located in the centre of multiple leaves, this method still has limitations. Overall, EEA still has advantages over SBF when segmenting leaves of varying complexity.

Table 6 evaluates the performance of the SBF and EEA algorithms in leaf segmentation. The table compares the average segmentation accuracy, recall, and f1-score of the two algorithms on cotton plants. The f1-score and accuracy of EEA are both higher than those of the SBF algorithm, with an average accuracy reaching 0.95 and an average f1-score reaching 0.94. In contrast, the average accuracy of the SBF algorithm only reached 0.85, and the f1-score was 0.92. The recall of SBF is slightly higher than EEA, which is due to the point offset when up-sampling and restoring leaves, resulting in a slight decrease in recall.

3.4. Phenotypic data evaluation

The accuracy of the extracted plant phenotypic traits was evaluated using the correlation coefficient R^2 and root mean square error (RMSE), as shown in Fig. 11. Twelve cotton plants, comprising a total of 302 leaves, were selected for comparison of segmentation results with manually measured and extracted traits.

In leaf area prediction, the R^2 value was 0.90, RRMSE was 0.19, and RMSE was 22.73, resulting in the identification of the optimal linear

prediction model. Utilizing the single leaf area, the canopy leaf area value was computed, resulting in an R^2 value of 0.99, RRMSE of 0.02, and RMSE of 37.07. These results further validate the effectiveness of leaf area prediction method based on the voxel approach.

In terms of plant height, the distance between the highest and lowest points was utilized, R^2 reached 0.99, RRMSE was 0.01, RMSE was 0.76. The number of leaves for each plant was calculated based on the segmentation results, yielding fairly accurate outcomes, R^2 reached 0.96, RRMSE was 0.04, RMSE was 0.50.

3.5. Measurement of wilt degree

During the seedling stage, plants affected by drought stress were identified through the observation of the wilting degree of plant leaves under various varieties and stress levels. According to criteria, plants with a wilting degree of less than 15% are considered to be in a normal state. As shown in Fig. 12A, during the emergence period under various moisture stress conditions, both varieties did not reach a wilting state, but quantitative data still revealed differences between the varieties. Therefore, during the seedling stage, the J2658 variety exhibited stronger drought resistance. Additionally, as observed in Fig. 12B, the degree of wilting gradually increased with the intensification of stress. The Jnd36 variety exhibited severe wilting under moderate and severe stress, while the J2658 variety performed well under all stress levels and did not reach the wilting degree. This further confirms that J2658 demonstrates strong drought resistance during the seedling stage.

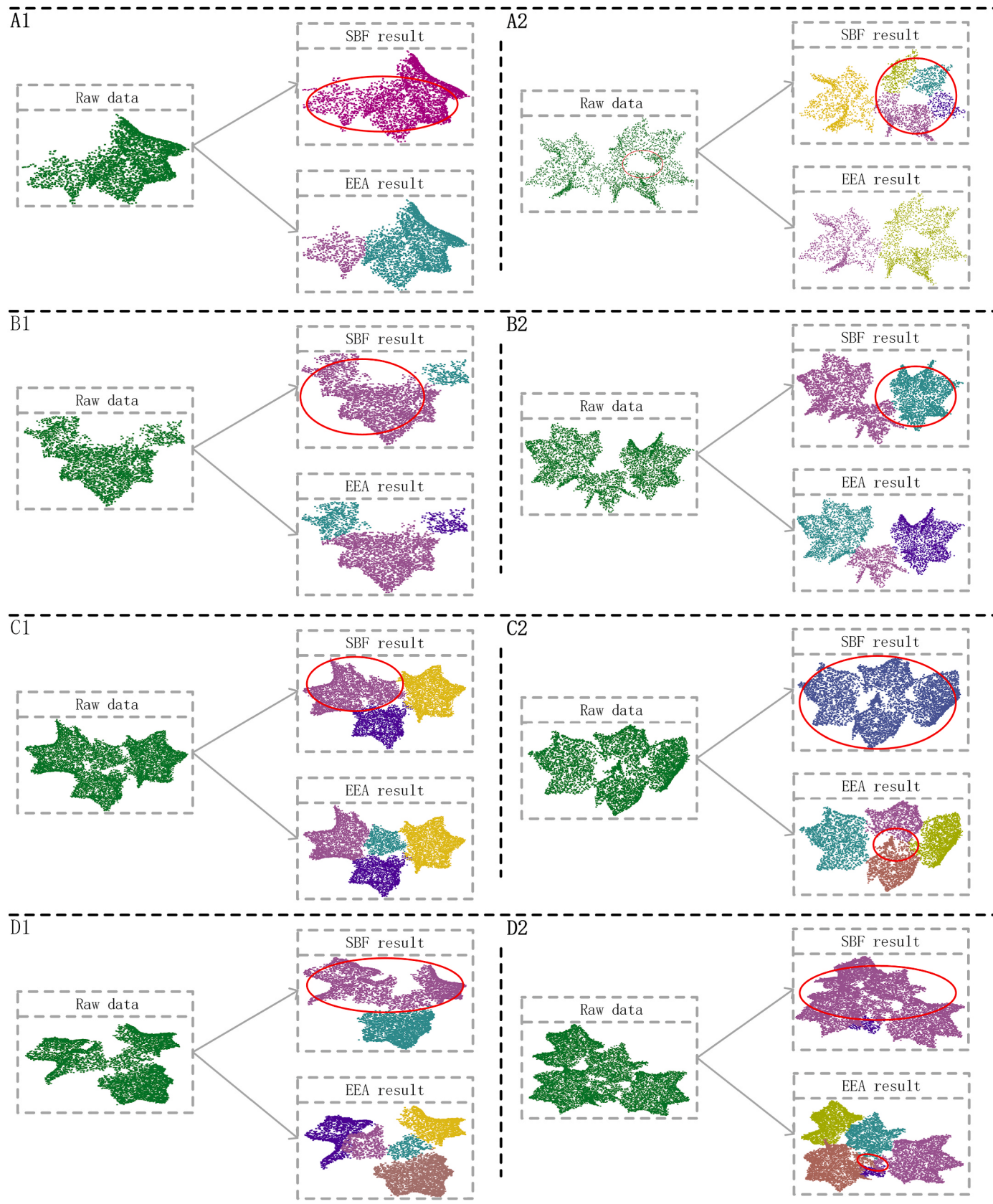


Fig. 10. Comparison of SBF and EEA results for overlapping blades of different complexity levels. A, B, C, and D denote the segmentation results for blades with complexity levels two, three, four, and five, respectively.

Table 6
Comparing the precision of complex blade segmentation.

Method EM	Predict	Recall	F1_score
SBF	0.89	0.96	0.92
EEA	0.95	0.93	0.94

Finally, at the bud stage, as shown in Fig. 12C, both varieties exhibited a wide range of wilting. Under mild, moderate, and severe stress, the wilting degree of J2658 was slightly lower than that of Jnd36. Therefore, even at the bud stage, J2658 still demonstrated higher drought resistance. In summary, based on the experimental results, the J2658 variety exhibited stronger drought resistance during the seedling and bud stages compared to the Jnd36 variety. These findings are of significant importance for further research and selection of cotton varieties with robust drought resistance.

3.6. Data analysis

As the wilting level of cotton plants at emergence and seedling stage is low or even not up to the standard of wilting, only the data at bud stage of cotton were used for data analysis. As shown in Fig. 13, four plants of each variety were selected as the analysed materials. The results of the algorithm can be found that cotton J2658 varieties are more

stable and drought-resistant under water stress than Jnd36 varieties. At the same time, with the intensification of water stress, the degree of wilt of Jnd36 varieties increased faster. This also indicates that cotton Jnd36 varieties are more sensitive to water stress, while the wilt degree of J2658 is relatively stable under different stress levels, indicating that J2658 varieties have stronger drought resistance. Through the analysis, we found that our method can quantify the wilting status of plants and provide quantitative reference data for the evaluation of plant drought resistance.

3.7. Cotton MVS software

Based on the methods mentioned above, a software system named Cotton MVS has been developed. The input of the software is raw point cloud data, and the output includes segmented stems, leaves, the completed segmentation of cotton plants, and the corresponding phenotype parameter files, as shown in Fig. 14. The software primarily consists of the menu bar, shortcut menu bar, display window, process display list, processing flow, and progress bar. The display window is used to show the processed cotton point cloud data, the process display list shows the processing progress, and the processing flow details the steps required by the algorithm. "data_pre" represents the pre-processing module, as shown in Fig. 14A, "Start Calculation" represents phenotype extraction, as demonstrated in Fig. 14B and C, showcasing the

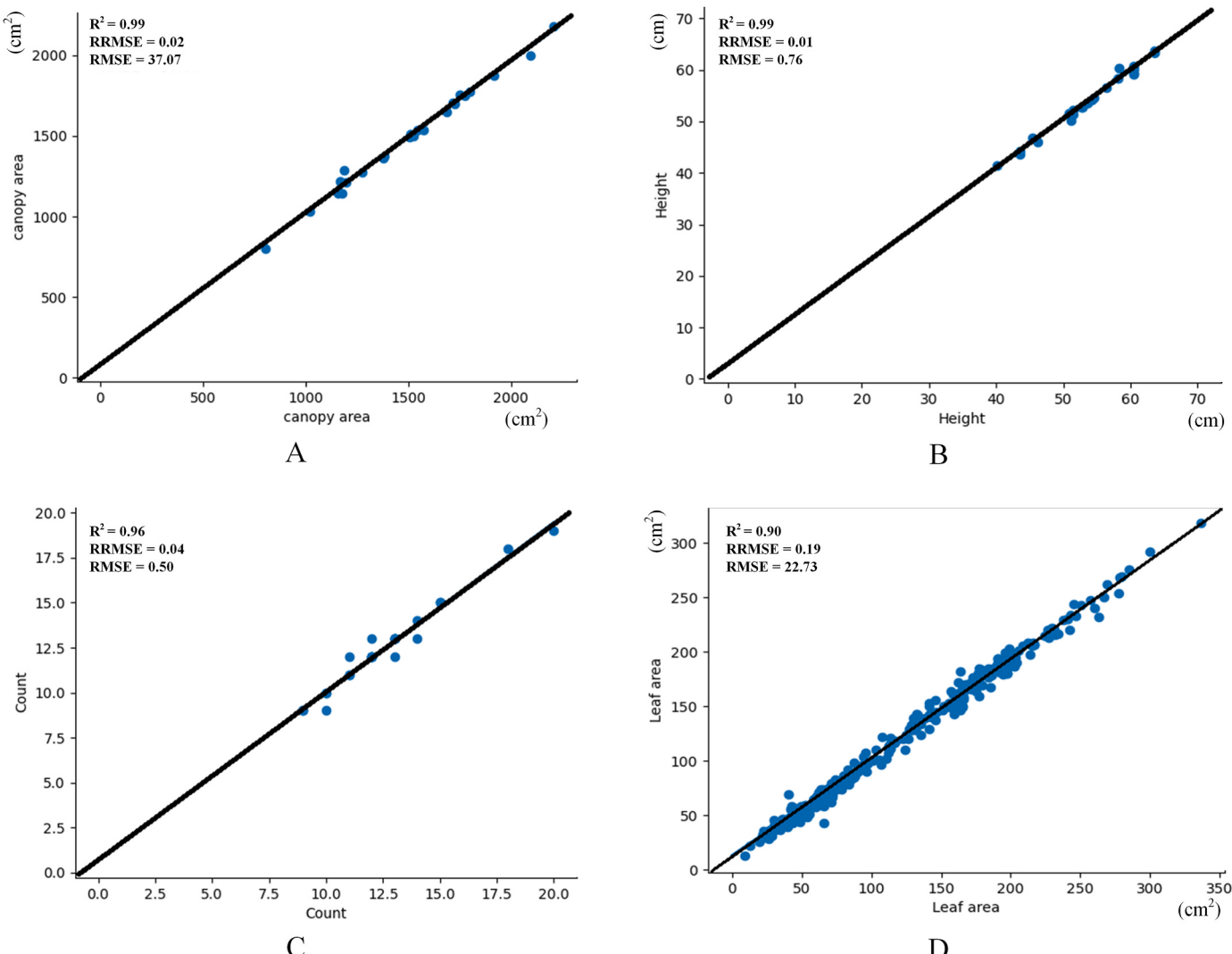


Fig. 11. Obtaining phenotype accuracy and error.

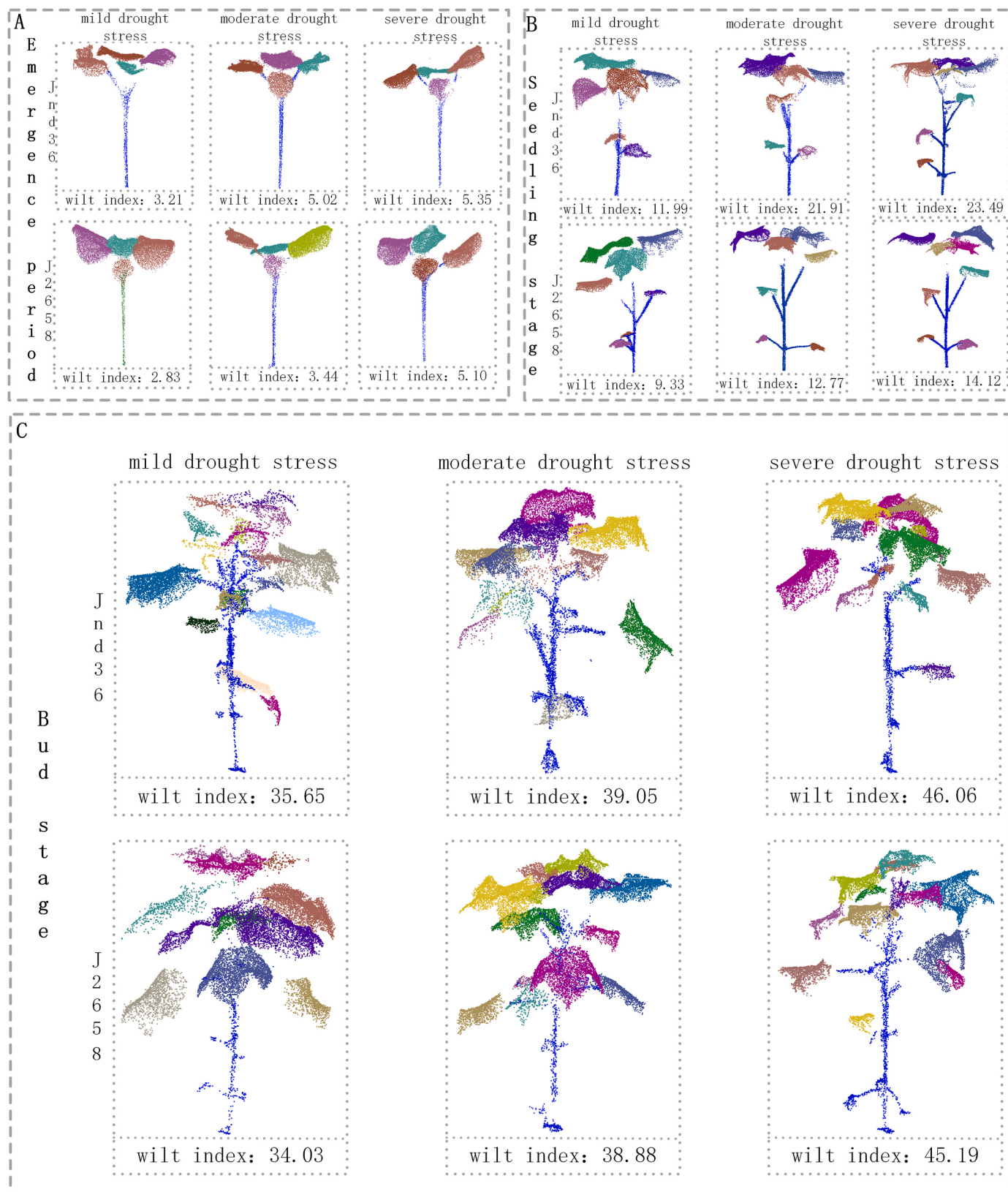


Fig. 12. Display of wilt severity in cotton plants of different varieties at different stages. A shows the condition during emergence, B shows the condition during seedling stage, and C shows the condition during flowering stage.

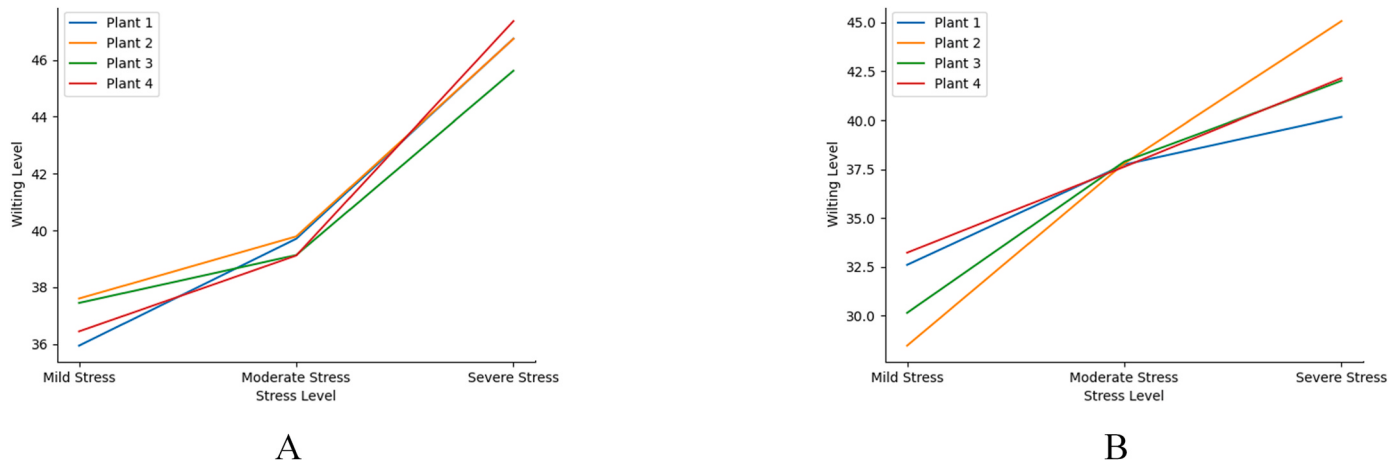


Fig. 13. Data analysis: A) Jnd36 variety and B) J2658 variety.

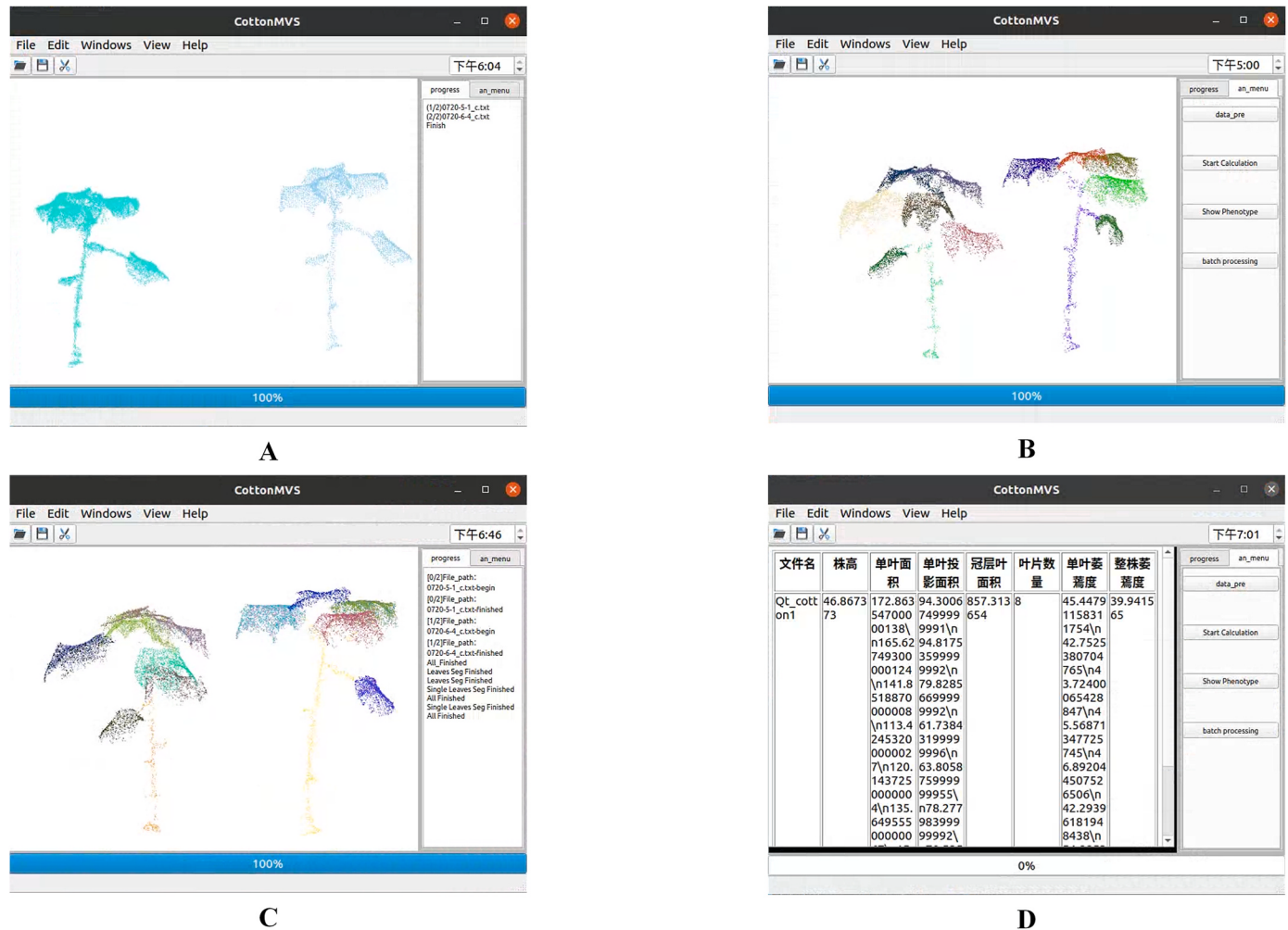


Fig. 14. Software interface and functionality diagram.

segmented cotton point cloud. "Show Phenotype" indicates phenotype display, as depicted in Fig. 14D, showing the phenotype parameter list, while "batch processing" represents batch processing operations. "progress" is used to display processing progress, and "an_menu" is used to display the processing flow. Testing was conducted on the point cloud data of 8 cotton plants, as shown in Table 7. The average time for 3D reconstruction was 89.75 min, data pre-processing took an average of

0.46 min, and phenotype extraction took an average of 3.9 min.

4. Discussion

This study aims to solve the problem of 3D reconstruction, segmentation and phenotype extraction of cotton plants to obtain richer phenotypic parameters. The experimental design uses a single cotton

Table 7

Efficiency evaluation of the software, where "Cotton" represents different cotton plants; "Data acquisition" indicates the time required for data acquisition, in minutes; "3D reconstruction" represents the time required for 3D reconstruction, in minutes; "Preprocessing" indicates the time required for data preprocessing, in minutes; "Phenotype extraction" represents the time required for phenotype extraction, in minutes.

Cotton	Data acquisition	3D reconstruction	Preprocessing	phenotype extraction
1	2	85	0.2	2.5
2	2	88	0.5	3.2
3	2	93	0.3	2.8
4	2	84	0.1	3
5	2	96	0.6	5.2
6	2	80	0.7	4.2
7	2	99	0.8	8.2
8	2	93	0.5	2.1
Mean	2	89.75	0.46	3.9

plant under water stress as a data resource. Previously, most of the cotton phenotyping studies were based on drones, LIDAR, etc. (Sun et al., 2021; Wu, Wen, Lan, et al., 2022; Xu et al., 2021), and the phenotypic data are less accessible, data collection is difficult, and field-grown cotton is well irrigated and does not wilt during growth, resulting in fewer compound leaves in this type of cotton (Saeed & Li, 2021). There is a relative paucity of literature examining the quantification of wilting levels, and in-depth exploration and analysis in this area remains to be undertaken. In the field of plant physiology and digital image processing, there is a lack of systematic methods and tools to accurately and reproducibly quantify the degree of wilting in plants. Therefore, it is crucial to conduct more research to fill this knowledge gap. The present study endeavours to address the above issues and to design the investigated methodology into software that is easy to follow.

By comparing various acquisition and reconstruction methods, a three-camera setup with a rotation speed of 30 was chosen for multi-view image acquisition. Compared to the Open MVS-PhenoV2 acquisition scheme proposed by (Wu, Wen, Lan, et al., 2022), the time required in this study increased by approximately 1 min. This is mainly due to the fact that the improved device is configured with three cameras and the cotton plants are relatively high, too fast turntable speed may cause shaking of the cameras and cotton plants, which in turn affects the reconstruction quality. For point cloud reconstruction, we chose the commercially available reconstruction software Context Capture, which offers higher advantages in terms of reconstruction time and reconstruction quality compared to OpenMVS (Cerneia, 2023). However, it is recognised that different setups may involve different resource requirements. Therefore, the pros and cons must be weighed on a case-by-case basis in practical applications.

Segmentation methods determine the accuracy of late phenotype acquisition. In terms of performance comparison of deep learning algorithms, The PointSegAt algorithm was adopted for plant segmentation tasks. It outperformed other comparative algorithms in terms of MIou and average accuracy. PointSegAt demonstrated excellent performance in both training and testing phases, particularly in handling specific challenges such as wilting and adhesion in cotton plants, maintaining high accuracy. Although DFSP (Wang et al., 2023) this method exhibits high precision and recall when dealing with a large number of maize samples, there are cases of over-segmentation, and for complex leaf segmentation precision is not high. The effectiveness of ABS throughout the cotton plant's lifecycle was demonstrated through leaf segmentation at different growth stages, yielding satisfactory results in the seedling, growth, and flowering stages (refer to Fig. 10). The area growth algorithm was used to segment leaves of varying complexity into simple, medium and complex structures. Compared to the SBF algorithm (see Fig. 11), the ABS maintains a high level of accuracy when dealing with overlapping leaves with holes, whereas the SBF algorithm exhibits severe mis-segmentation. Although the ABS exhibits some

mis-segmentation when dealing with particularly complex blade structures (shown in Fig. 15), especially incomplete blades located at the centre of multiple blades, overall, the ABS still has an advantage over the SBF in blade complexity segmentation. On the contrary, although the SBF algorithm (Li et al., 2019) effectively solves the problem of complex blade segmentation, it cannot automatically identify complex blades and has low segmentation accuracy. Deep learning-based instance segmentation networks (Li, Wen, et al., 2022; Schunck et al., 2021; Wang et al., 2022) also suffered from poor accuracy and inaccurate identification in dealing with the complex blade problem, although the deep learning-based method has higher efficiency. During leaf segmentation, small leaves with fewer than 500 points were excluded, establishing a robust foundation for subsequent wilting degree determination. This indicates that ABS can effectively handle the morphological variations of cotton leaves at different growth stages. Although ABS performed well in the leaf segmentation task, it still has limitations when dealing with highly complex leaf structures such as incomplete leaves located at the centre of multiple plants. This suggests that future research could explore more complex segmentation strategies to enhance the adaptability of the algorithm to challenging scenarios. In addition, to address the point bias problem that affects recall, we need to explore finer up-sampling and recovery strategies to improve the overall performance of the algorithm in a comprehensive manner.

There are more existing methods for crop phenotype extraction, (Masuda, 2021) performed leaf area estimation by the number of leaf dots around the leaf, and (Itakura & Hosoi, 2018) performed an accurate calculation of leaf area by means of a voxel-based approach. A voxel-based approach is used to predict leaf area and its effectiveness is demonstrated by comparing the results with manual measurements. Satisfactory results were achieved for the metrics of R^2 and RMSE for leaf area, plant height and number of leaves when compared to manual measurements. This provides a viable method for phenotypic measurements of a large number of plants using drones or other remote sensing methods. In this study, a wilting degree measure was designed to quantify the degree of wilting, which could be effective in avoiding water stress on cotton plants, which proves the significance of this study as quantification of wilting degree is lacking in previous studies.

The method has the following limitations: for special complex blade processing is still not ideal (Fig. 15), due to the blade overlap is too serious, the use of ABS method can not be divided in fewer iterations to complete, and its impact on the efficiency, so for special complex blade processing the algorithm is still lacking; ABS exists in multiple iterations and edge corrosion, so in the efficiency is lower as shown in Table 7. Therefore, future research should be improved in solving the special complex blades and the efficiency of the algorithm.

5. Conclusion

Combined with the results obtained in multi-view image acquisition, deep learning algorithms, leaf segmentation, plant phenotypic feature extraction, and the effects of drought stress, this research has made significant progress. For multi-view image acquisition, a three-camera setup with a rotation speed of 30 was chosen and a contextual capture technique was used for 3D reconstruction, which played an important role in improving the quality of the data. The PointSegAt algorithm performed well in the plant segmentation task, but there are still challenges in terms of computational efficiency, which is an area that can be focused on in future research. The leaf segmentation method performs well in different growth stages and leaf structures, but still has limitations in particularly complex structures and needs further optimisation.

The leaf area prediction model based on the voxel method yielded satisfactory results and provided a feasible method for phenotypic measurements of a large number of plant populations. Observations on different cotton varieties under drought stress provided a scientific basis for breeding drought-resistant varieties. The developed cotton MVS software is a practical tool for plant image data processing, and future

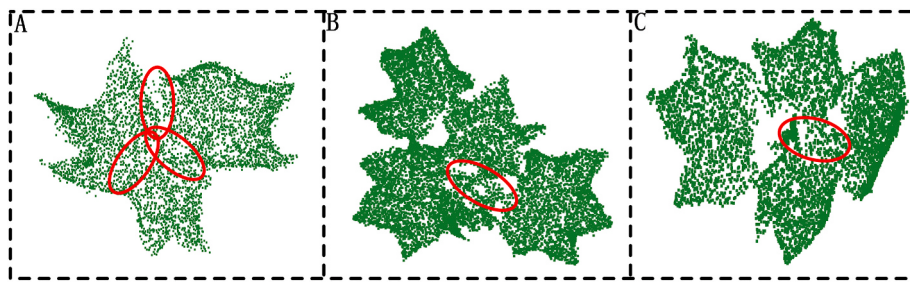


Fig. 15. Display of extremely complex leaves, with A, B, and C representing three different scenarios.

research will continue to optimise the methodology and tools, expand its application scope, and contribute more useful results to the field of plant science.

Funding

This work was partially supported by National Key R&D Program of China(2022ZD0115801),Beijing Academy of Agricultural and Forestry Sciences Youth Research Fund of China(QNJJ202229),Construction of Collaborative Innovation Center of Beijing Academy of Agricultural and Forestry Sciences (KJCX201917), Natural Science Foundation of Guangdong Province (2022B1515120059), National Natural Science Foundation of China(grant numbers 61871475), Research on precise control algorithms for waterfowl breeding based on artificial intelligence and data-driven(KJCX2022018).

Declaration of competing interest

The authors declare that they have no known competing financial interests or personal relationships that could have appeared to influence the work reported in this paper.

References

- Aslam, S., Hussain, S. B., Baber, M., Shaheen, S., Aslam, S., Waheed, R., Seo, H., & Azhar, M. T. (2023). Estimation of drought tolerance indices in upland cotton under water deficit conditions. *Agronomy*, 13(4), 984. <https://doi.org/10.3390/agronomy13040984>
- Barazzetti, L. (2018). Point cloud occlusion recovery with shallow feedforward neural networks. *Advanced Engineering Informatics*, 38, 605–619. <https://doi.org/10.1016/j.aei.2018.09.007>
- Cerneia, D. OpenMVS: Open Multiple View Stereovision. Available online: <https://github.com/cdcseacave/openMVS/> (accessed on 18 November 2023).
- Chandell, N. S., Chakraborty, S. K., Rajwade, Y. A., Dubey, K., Tiwari, M. K., & Jat, D. (2021). Identifying crop water stress using deep learning models. *Neural Computing & Applications*, 33, 5353–5367. <https://doi.org/10.1007/s00521-020-05325-4>
- Chang, L., Fan, H., Zhu, N., & Dong, Z. (2022a). A two-stage approach for individual tree segmentation from TLS point clouds. *IEEE Journal of Selected Topics in Applied Earth Observations and Remote Sensing*, 15, 8682–8693. <https://doi.org/10.1109/JSTARS.2022.3212445>
- Chen, H., Wei, Z., Xu, Y., Wei, M., & Wang, J. (2022b). Imlovenet: Misaligned image-supported registration network for low-overlap point cloud pairs. In *ACM SIGGRAPH 2022 conference proceedings* (pp. 1–9). <https://doi.org/10.1145/3528233.3530744>
- Das Choudhury, S., Saha, S., Samal, A., Mazis, A., & Awada, T. (2023). Drought stress prediction and propagation using time series modeling on multimodal plant image sequences. *Frontiers in Plant Science*, 14, 1003150. <https://doi.org/10.3389/fpls.2023.1003150>
- Engel, N., Belagiannis, V., & Dietmayer, K. (2021). Point transformer. *IEEE access*, 9, 134826–134840. <https://doi.org/10.1109/ACCESS.2021.3116304>
- Gill, T., Gill, S. K., Saini, D. K., Chopra, Y., de Koff, J. P., & Sandhu, K. S. (2022). A comprehensive review of high throughput phenotyping and machine learning for plant stress phenotyping. *Phenomics*, 2(3), 156–183. <https://doi.org/10.1007/s43657-022-00048-z>
- Girardeau-Montaut, D. (2016). CloudCompare. France: EDF R&D Telecom ParisTech, 11, 5.
- Hirt, P. R., Holtkamp, J., Hoegner, L., Xu, Y., & Stilla, U. (2022). Occlusion detection of traffic signs by voxel-based ray tracing using highly detailed models and MLS point clouds of vegetation. *International Journal of Applied Earth Observation and Geoinformation*, 114, 103017. <https://doi.org/10.1016/j.jag.2022.103017>
- Itakura, K., & Hosoi, F. (2018). Automatic leaf segmentation for estimating leaf area and leaf inclination angle in 3D plant images. *Sensors*, 18(10), 3576. <https://doi.org/10.3390/s18103576>
- Jiang, Y., Li, C., Robertson, J. S., Sun, S., Xu, R., & Paterson, A. H. (2018). GPhenoVision: A ground mobile system with multi-modal imaging for field-based high throughput phenotyping of cotton. *Scientific Reports*, 8(1), 1213. <https://doi.org/10.1038/s41598-018-19142-2>
- Jiang, Y., Li, C., Xu, R., Sun, S., Robertson, J. S., & Paterson, A. H. (2020). DeepFlower: A deep learning-based approach to characterize flowering patterns of cotton plants in the field. *Plant Methods*, 16(1), 1–17.
- Laxman, R. H., Hemamalini, P., Namratha, M. R., Bhatt, R. M., & Sadashiva, A. T. (2022). Phenotyping deficit moisture stress tolerance in tomato using image derived digital features. *International Journal of Bio-resource and Stress Management*, 13(4), 339–347. <https://doi.org/10.1007/s00521-020-05325-4>
- Li, D., Cao, Y., Shi, G., Cai, X., Chen, Y., Wang, S., & Yan, S. (2019). An overlapping-free leaf segmentation method for plant point clouds. *IEEE Access*, 7, 129054–129070. <https://doi.org/10.1109/ACCESS.2019.2940385>
- Li, D., Li, J., Xiang, S., & Pan, A. (2022a). PSegNet: Simultaneous semantic and instance segmentation for point clouds of plants. *Plant Phenomics*. <https://doi.org/10.34133/2022/9787643>
- Li, J., Schachtman, D. P., Creech, C. F., Wang, L., Ge, Y., & Shi, Y. (2022b). Evaluation of UAV-derived multimodal remote sensing data for biomass prediction and drought tolerance assessment in bioenergy sorghum. *The Crop Journal*, 10(5), 1363–1375. <https://doi.org/10.1016/j.cj.2022.04.005>
- Li, R., Liu, Y., Yang, M., et al. (2018). Three-dimensional point cloud segmentation algorithm based on improved region growing[J]. *Laser & Optoelectronics Progress*, 55(5), Article 051502. <https://doi.org/10.3788/LOP5.051502>
- Li, Y., Wen, W., Miao, T., Wu, S., Yu, Z., Wang, X., ... Zhao, C. (2022c). Automatic organ-level point cloud segmentation of maize shoots by integrating high-throughput data acquisition and deep learning. *Computers and Electronics in Agriculture*, 193, 106702. <https://doi.org/10.1016/j.compag.2022.106702>
- Lin, S., Xiu, Y., Kong, J., Yang, C., & Zhao, C. (2023). An effective pyramid neural network based on graph-related attentions structure for fine-grained disease and pest identification in intelligent agriculture. *Agriculture*, 13(3), 567. <https://doi.org/10.3390/agriculture13030567>
- Liu, X., Hu, C., & Li, P. (2020). Automatic segmentation of overlapped poplar seedling leaves combining Mask R-CNN and DBSCAN. *Computers and Electronics in Agriculture*, 178, 105753. <https://doi.org/10.1016/j.compag.2020.105753>
- Masuda, T. (2021). Leaf area estimation by semantic segmentation of point cloud of tomato plants. In *Proceedings of the IEEE/CVF international conference on computer vision* (pp. 1381–1389).
- Miao, T., Wen, W., Li, Y., Wu, S., Zhu, C., & Guo, X. (2021). Label3DMaize: Toolkit for 3D point cloud data annotation of maize shoots. *GigaScience*, 10(5). <https://doi.org/10.1093/gigascience/giab031>.
- Novel, C., Keriven, R., Graindorge, P., & Poux, F. (2016). A bentley systems white paper.
- Qi, C. R., Su, H., Mo, K., & Guibas, L. J. (2017a). Pointnet: Deep learning on point sets for 3d classification and segmentation. In *In Proceedings of the IEEE conference on computer vision and pattern recognition* (pp. 652–660).
- Qi, C. R., Yi, L., Su, H., & Guibas, L. J. (2017b). Pointnet++: Deep hierarchical feature learning on point sets in a metric space. *Advances in Neural Information Processing Systems*, 30.
- Qiu, R., Miao, Y., Zhang, M., & Li, H. (2021). Detection of the 3D temperature characteristics of maize under water stress using thermal and RGB-D cameras. *Computers and Electronics in Agriculture*, 191, 106551. <https://doi.org/10.1016/j.compag.2021.106551>
- Ramamoorthy, P., Samiappan, S., Wubben, M. J., Brooks, J. P., Shrestha, A., Panda, R. M., ... Bheemanahalli, R. (2022). Hyperspectral reflectance and machine learning approaches for the detection of drought and root-knot nematode infestation in cotton. *Remote Sensing*, 14(16), 4021. <https://doi.org/10.3390/rs14164021>
- Saeed, F., & Li, C. (2021). Plant organ segmentation from point clouds using Point-Voxel CNN. In *2021 ASABE annual international virtual meeting* (p. 1). American Society of Agricultural and Biological Engineers. <https://doi.org/10.13031/aim.202100428>
- Sarkar, S., Ramsey, A. F., Cazenave, A. B., & Balota, M. (2021). Peanut leaf wilting estimation from RGB color indices and logistic models. *Frontiers of Plant Science*, 12, 658621. <https://doi.org/10.3389/fpls.2021.658621>
- Schunck, D., Magistri, F., Rosu, R. A., Cornelisen, A., Chebrolu, N., Paulus, S., ... Klingbeil, L. (2021). Pheno4D: A spatio-temporal dataset of maize and tomato plant point clouds for phenotypic analysis. *PLoS One*, 16(8), Article e0256340. <https://doi.org/10.1371/journal.pone.0256340>
- Sun, S., Li, C., Chee, P. W., Paterson, A. H., Meng, C., Zhang, J., ... Adhikari, J. (2021). High resolution 3D terrestrial LiDAR for cotton plant main stalk and node detection.

- Computers and Electronics in Agriculture*, 187, 106276. <https://doi.org/10.1016/j.compag.2021.106276>
- Thomas, H., Qi, C. R., Deschaud, J. E., Marcotegui, B., Goulette, F., & Guibas, L. J. (2019). Kpconv: Flexible and deformable convolution for point clouds. In *Proceedings of the IEEE/CVF international conference on computer vision* (pp. 6411–6420).
- Vo, A. V., Truong-Hong, L., Laefer, D. F., & Bertolotto, M. (2015). Octree-based region growing for point cloud segmentation. *ISPRS Journal of Photogrammetry and Remote Sensing*, 104, 88–100. <https://doi.org/10.1016/j.isprsjprs.2015.01.011>
- Wang, H., Liu, Q., Yue, X., Lasenby, J., & Kusner, M. J. (2021). Unsupervised point cloud pre-training via occlusion completion. In *In Proceedings of the IEEE/CVF international conference on computer vision* (pp. 9782–9792).
- Wang, D., Song, Z., Miao, T., Zhu, C., Yang, X., Yang, T., ... Xu, T. (2023). Dfsp: A fast and automatic distance field-based stem-leaf segmentation pipeline for point cloud of maize shoot. *Frontiers in Plant Science*, 14, 1109314. <https://doi.org/10.3389/fpls.2023.1109314>
- Wang, L., Zheng, L., & Wang, M. (2022). 3D point cloud instance segmentation of lettuce based on PartNet. In *Proceedings of the IEEE/CVF conference on computer vision and pattern recognition* (pp. 1647–1655).
- Wu, S., Wen, W., Gou, W., Lu, X., Zhang, W., Zheng, C., ... Guo, X. (2022a). A miniaturized phenotyping platform for individual plants using multi-view stereo 3D reconstruction. *Frontiers in Plant Science*, 13, 897746. <https://doi.org/10.3389/fpls.2022.897746>
- Wu, J., Wen, S., Lan, Y., Yin, X., Zhang, J., & Ge, Y. (2022b). Estimation of cotton canopy parameters based on unmanned aerial vehicle (UAV) oblique photography. *Plant Methods*, 18(1), 129. <https://doi.org/10.21203/rs.3.rs-2179960/v1>
- Xiao, J., Zhang, J., Adler, B., Zhang, H., & Zhang, J. (2013). Three-dimensional point cloud plane segmentation in both structured and unstructured environments.
- Robotics and Autonomous Systems*, 61(12), 1641–1652. <https://doi.org/10.1016/j.robot.2013.07.001>
- Xu, Y. A. N. G., Songtao, H. U., Yinghua, W. A. N. G., Wanneng, Y. A. N. G., & Ruifang, Z. H. A. I. (2021). Cotton phenotypic trait extraction using multi-temporal laser point clouds. *Smart Agriculture*, 3(1), 51. <https://doi.org/10.12133/j.smartag.2021.3.1.202102-SA003>
- Yang, M., Huang, C., Kang, X., Qin, S., Ma, L., Wang, J., ... Zhang, Z. (2022). Early monitoring of cotton verticillium wilt by leaf multiple “symptom” characteristics. *Remote Sensing*, 14(20), 5241. <https://doi.org/10.3390/rs14205241>
- Zhang, M., Chen, T. E., Gu, X., Chen, D., Wang, C., Wu, W., ... Zhao, C. (2023). Hyperspectral remote sensing for tobacco quality estimation, yield prediction, and stress detection: A review of applications and methods. *Frontiers in Plant Science*, 14, 1073346. <https://doi.org/10.3389/fpls.2023.1073346>
- Zhao, J., Pan, F., Li, Z., Lan, Y., Lu, L., Yang, D., & Wen, Y. (2021). Detection of cotton waterlogging stress based on hyperspectral images and convolutional neural network. *International Journal of Agricultural and Biological Engineering*, 14(2), 167–174.
- Zhou, Y., Lao, C., Yang, Y., Zhang, Z., Chen, H., Chen, Y., ... Yang, N. (2021a). Diagnosis of winter-wheat water stress based on UAV-borne multispectral image texture and vegetation indices. *Agricultural Water Management*, 256, 107076. <https://doi.org/10.1016/j.agwat.2021.107076>
- Zhou, J., Zhou, J., Ye, H., Ali, M. L., Chen, P., & Nguyen, H. T. (2021b). Yield estimation of soybean breeding lines under drought stress using unmanned aerial vehicle-based imagery and convolutional neural network. *Biosystems Engineering*, 204, 90–103. <https://doi.org/10.1016/j.biosystemseng.2021.01.017>